Modelling of Thermal Wave Propagation in Damaged Composites with Internal Source

[1]Francesco Ciampa, [1]Stefano L. Angioni, [1]Fulvio Pinto, [2]Gennaro Scarselli, [1]Darrel P. Almond, [1]Michele Meo

[1]Department of Mechanical Engineering, University of Bath, BA2 7AY, Bath, UK

[2]Department of Engineering for Innovation, University of Salento, 73100, Lecce, Italy

ABSTRACT

SMArt Thermography exploits the electrothermal properties of multifunctional smart structures, which are created by embedding shape memory alloy (SMA) wires in traditional carbon fibre reinforced composite laminates (known as SMArt composites), in order to detect the structural flaws using an embedded source. Such a system enables a built-in, fast, cost-effective and in-depth assessment of the structural damage as it overcomes the limitations of standard thermography techniques. However, a theoretical background of the thermal wave propagation behaviour, especially in the presence of internal structural defects, is needed to better interpret the observations/data acquired during the experiments and to optimise those critical parameters such as the mechanical and thermal properties of the composite laminate, the depth of the SMA wires and the intensity of the excitation energy. This information is essential to enhance the sensitivity of the system, thus to evaluate the integrity of the medium with different types of damage. For this purpose, this paper aims at developing an analytical model for SMArt composites, which is able to predict the temperature contrast on the surface of the laminate in the presence of in-plane internal damage (delamination-like) using pulsed thermography. Such a model, based on the Green's function formalism for one-dimensional heat equation, takes into account the thermal lateral diffusion around the defect and it can be used to compute the defect depth within the laminate. The results showed good agreement between the analytical model and the measured thermal waves using an infrared (IR) camera. Particularly, the contrast temperature curves were found to change significantly depending on the defect opening.

Keywords: *composite materials, pulsed thermography, shape memory allow wires, defect depth*

1. INTRODUCTION

The non-destructive evaluation (NDE) testing of composite structures becomes more important and demanding as composite materials are increasingly used in safety critical applications, such as aircraft primary structures or as means to transport corrosive fluids in the oil and gas industry. Flash or pulsed thermography is the most commonly used thermographic NDE technique for the assessment of subsurface defects in composites [1, 2]. Indeed, detection of delamination defects between plies can significantly reduce the strength and performance of composite structures under compressive in-plane loading, eventually giving rise after bucking to global plate instability [3, 4, 5].

Pulsed thermography uses optical flash excitation in which a brief controlled thermal stimulation pulse is applied to the surface of the part under investigation at the beginning of the test [6]. The result is an instantaneous rise in temperature of the surface followed by a rapid cooling monitored by an infrared (IR) camera. The video images are then stored in a personal computer (PC) for viewing at the end of the test. Since thermal waves flow inside the sample by diffusion, the heat diffusion rate over a structural defect will differ with reference to the surrounding area. Hence, the resulting thermal response can be employed to quantify the internal state of the materials. The use of flash thermography to retrieve the defect size from the thermal images has been performed employing both analytical, experimental and numerical techniques [7, 8, 9]. An analytical model for flash thermography has been developed in [10], which has been found to provide good

results when compared against both experimental and finite difference simulations [11]. This model is based on the impulse heating transient response of an adiabatically isolated layer [12, 13] where the thermal response function of the layer is given by the thermal wave interference expression obtained in Bennett and Patty [14]. However, flash thermography presents a series of complications caused by the use of external sources such as high-power photographic flashes or infrared radiators. As an example, the positioning of the lamp(s) from the part under inspection can have a significant impact on the resulting thermal response. Also, the optical characteristics of the surface of the material or its coating heavily impact the results of the inspection. Many materials are translucent, i.e. light is absorbed in them over a range of depths (and consequently the heat source obtained by flash excitation is not confined to the surface; it is distributed over a range of depths), but their optical absorption coefficients are not readily available.

In this paper a novel approach to pulsed thermography, which does not require external lamps, but is instead based on SMArt composites, is considered. A SMArt composite is a new kind of multifunctional material obtained by embedding SMA wires within traditional CFRP composites [15]. Multifunctional materials lead to optimal system performance, by combining different functions into a single material, otherwise not possible through independent subsystem optimisation [16]. Specifically, the embodiment of SMA within the lay-up of CFRP laminates has been widely studied as a valid manufacturing procedure to enhance the impact resistance of traditional composite structures due to their unique physical properties such as shape memory effect and superelasticity [17]. The electrical variation of embedded SMA wires to the strain distribution within hybrid glass fibre reinforced plastic (GFRP) laminates has been correlated by Nagai and Oishi [18], while a hybrid CFRP/SMA composite with damages suppression function that is enabled by activating the martensite-austenite transformation was manufactured by Xu et al. [19]. However, to date, only few works have investigated the possibility of exploiting the presence of an internal hybrid grid to enable the laminate to have multiple additional features, hence resulting in a real multifunctional system characterized by specific properties that go further than the traditional load-bearing functionality. Based on these premises, a SMA based multi-functional composite (named SMArt) was developed exploiting their intrinsic thermoelectric properties for applications such as sensing, thermography and de-icing [20]. In particular SMArt thermography is a form of material enabled thermography where the embedded SMA wires are used as heat sources to generate in situ power resistive heating (ohmic heating or joule heating) that can be used to perform pulsed thermography [21]. Although good results in term of damage detection have been already obtained with this new technique, there is still the need for a rigorous theoretical frame in which this phenomenon must be included. Such a model should not be limited to the inclusion of SMA, but should be extendable to any kind of conductive wire embedded into the traditional lay-up of a composite laminate.

In this paper an analytical model for pulsed thermography using SMArt composites will be developed specifically for in-plane, delamination-like defects. This model can be used to predict the temperature contrast on the surface of the laminate, accounting for (i) defect depth, size and opening, (ii) thermal properties of material and defect filler, (iii) thickness of the component, (iv) depth of the SMA wire and intensity of the excitation energy. Moreover, using this model an analytical expression for evaluating the defect depth will be obtained. Finally, the results of the analytical model and defect depth evaluation are contrasted against experimental results. The layout of the paper is as follows: Section 2 describes the theory behind the analytical model and its application to evaluating analytically the defect depth, while Section 3 compares the model against some experimental data. Section 4 provides some conclusions from this work and summarises the major findings.

2. ANALYTICAL MODEL

For the analytical model, an SMA wire is embedded at a depth h in a composite laminated plate of thickness L. By transmitting an impulse of resistive heating through the wire, it is possible to identify the presence of a defect using infrared imaging of the variations of the temperature contrast on the surface of the composite laminate. Here we are assuming an in-plane, delamination-like circular defect of diameter D at a depth d from the surface of the material, as described in figure (1).

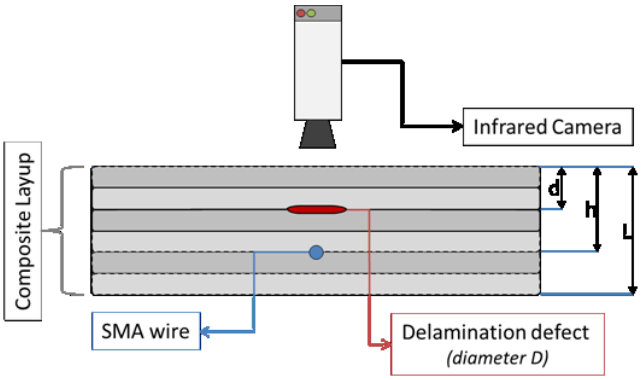

Figure 1 Identification of an in-plane, delamination-like, circular defect in a composite laminate through pulsed thermography using an SMA wire as heat source.

Consider the laminated composite plate shown in the above figure, in which the origin of the coordinate system is placed at the centre of the SMA wire, which will be assumed to all effects and purposes to act as a line source. The components of the Cartesian coordinates are (x, y, z) where x, y are in-plane coordinates, and z is the transverse (out-of-plane) coordinate. Furthermore, it is assumed that the SMA wire runs along the y-axis. The three-dimensional inhomogeneous linear problem of finding the temperature field $T(\mathbf{r},t)$, which results from the transient heat conduction within the composite laminate due to an internal heat source $g(\mathbf{r},t)$ is given in Eq. (1):

$$\frac{1}{\alpha}\frac{\partial T(\mathbf{r},t)}{\partial t} - \nabla^2 T(\mathbf{r},t) = \frac{g(\mathbf{r},t)}{k} \quad \Omega \times (0,\infty) \quad t > 0, \tag{1}$$

where $\mathbf{r} = x\hat{i} + y\hat{j} + z\hat{n}$, $\Omega \subset \Re^2$ is the *domain of influence* and $\nabla^2 = \left(\frac{\partial^2}{\partial x^2}\hat{i} + \frac{\partial^2}{\partial y^2}\hat{j} + \frac{\partial^2}{\partial z^2}\hat{n}\right)$ is the Laplacian operator. In Eq. (1) k represents the thermal conductivity (Wm^{-1} K^{-1}), whilst $\alpha = k/\rho c$ is the thermal diffusivity (m^2 s^{-1}), with ρ and c the density (kg m^{-3}) and the specific heat (J kg^{-1} K^{-1}) of the composite material, respectively. The internal heat generation is due to the low power resistive heating (Joule effect) applied on the SMA wire. Since the heat equation is second order in space and first order in time, to have a well-posed problem, two boundary conditions and one initial condition must be specified. The initial condition is:

$$T(\mathbf{r},t_0) = 0\,. \tag{2}$$

In addition, assuming that there is no heat flow out of the edges of the laminate, the following boundary conditions (Dirichlet) can be used:

$$T(\mathbf{r},t) = 0 \quad S \times (0,\infty) \quad t > 0, \tag{3}$$

where S is the boundary of the composite laminate. After resistive heating, if a uniform impulse of thermal energy is released by the SMA wire as an instantaneous line source at time t = 0 and x = z = 0 along the y-axis (per unit length) of strength Q_0 (J m^{-1}), then it is well-known (e. g. [22]) that the temperature is independent of y and the corresponding fundamental solution is given as:

$$T(r,t) = \frac{Q_0}{4\pi k t} e^{-\frac{r^2}{4\alpha t}}, \tag{4}$$

where $r = \sqrt{x^2 + z^2}$ and $T(r,t)$ is the temperature rise at a distance *r* from the SMA wire at a time *t* after the impulse of heat energy has been released. We are interested in the cross-sectional propagation of the transient thermal wave (i.e. along the *z*-axis), so the corresponding one-dimensional (1D) field solution of the problem (1) is independent of *x* and *y*. When there is no defect in the component being inspected the heat released by the SMA wire will propagate straight through the laminated composite plate without impediments causing over time a temperature rise on the surface at a distance *h* from the wire. The temperature rise $T_{nd}(h,t)$ on the surface of the non-defective material will consist of two contributions. The first contribution $T_{nd}^{F}(h,t)$ is constituted by the *forward wave*, which reaches directly the surface, and all its subsequent reflections at the back face of the laminate of thickness *L*. The second one $T_{nd}^{R}(h,t)$, instead, is composed by the reverse wave, which reaches the surface only after being reflected at the back face of the laminate, and all its subsequent reflections by the same back face. Note that in theory there are an infinite number of reverberations, but in practice a summation over the first six terms is adequate. The 1D analytical model of the temperature rise (or background temperature) on the surface of the non-defective material $T_{nd}(h,t)$ is given by:

$$T_{nd}(h,t) = T_{nd}^{F}(h,t) + T_{nd}^{R}(h,t) = \frac{Q_0}{4\pi k t}\left[\sum_{m=0}^{\infty} e^{-\frac{(2mL+h)^2}{4\alpha t}} + \sum_{m=0}^{\infty} e^{-\frac{[2(m+1)L-h]^2}{4\alpha t}}\right]. \quad (5)$$

Note that the in Eq. (5) the magnitude of the heating produced at the surface varies inversely with the thermal conductivity *k* of the composite material being impulse heated and that this heat decays with time *t*. As a delamination-like defect lying beneath the surface in a plane parallel to the surface is being considered [see figure (1)], then both the magnitude and the time dependence of the temperature rise on the laminate surface, $T(h,t)$, will be altered by the defect, as the conduction of the heat released by the SMA wire to the surface will be reduced or blocked by the defect causing a slower temperature rise as indicated by Eq. (5). This results in the area of the surface over a defect appearing cooler in the IR video images collected during the test, thus enabling the detection of the defect.

As a first approximation, a region containing a delamination-like defect can be treated as a layer of thickness *d*, the depth of the defect, below the surface. When a defect is present in the component under inspection, a part Γ of the heat, generated by the SMA wire and being conducted towards the surface will be blocked by the defect, where Γ is the *effective thermal reflectivity* of the defect, assumed 100% for a wide open defect. This applies to both direct and reverse waves and all their reflections. Then only a fraction $(1-\Gamma)$ of the heat will therefore be able to reach the surface. Another fraction Γ of this heat reverberates at the surface after being reflected by the defect having a round-trip path of length 2*d*, with following terms having round-trip path lengths of 4*d*, 6*d*, etc. The 1D analytical model of the temperature rise $T_d(h,t)$ on the surface of the defective material is then given by the following equation:

$$T_d(h,t) = T_d^{F}(h,t) + T_d^{R}(h,t) =$$
$$\frac{Q_0}{4\pi k t}\left[\sum_{m=0}^{\infty}(1-\Gamma)^{2m+1}\sum_{m=0}^{\infty}\Gamma^n e^{-\frac{(2mL+h+2nd)^2}{4\alpha t}} + \sum_{m=0}^{\infty}(1-\Gamma)^{2m+1}\sum_{m=0}^{\infty} e^{-\frac{[2(m+1)L-h+2nd]^2}{4\alpha t}}\right]. \quad (6)$$

Real defects are not in finite in size, but are finite in their lateral dimensions, so heat flowing in their vicinity cannot be assumed to be a 1D phenomenon. As a circular defect of diameter *D* has been assumed, then the thermal lateral diffusion around the defect will also contribute to the defective temperature rise over time on the surface of the plate [10]. The physical assumption here is that the lateral diffusion of heat from the edge of the defect to the center will cause an increase with time in the temperature on the surface of the laminate over

the center of a defect. For a circular defect of diameter D, the diffusion distance is $D/2$. Accounting for lateral diffusion, then the temperature rise on the surface of the defect material [Eq. (6)] can be rewritten as:

$$T_{d1}(h,t) = T_d(h,t) + \left[T_{nd}(h,t) - T_d(h,t)\right] e^{-\frac{(D/2)^2}{4\alpha A t}}, \qquad (7)$$

where A is the *thermal diffusivity anisotropy* of the composite material. This type of anisotropy assumes a prominent importance on the temperature contrast caused by defects for materials that are thermally anisotropic, such as composites, for which in-plane thermal conductivity typically exceeds through-the-thickness conductivity because of the layered structure of composites. For this reason, the in-plane thermal diffusivity of composites is larger by a factor of $\approx 3-5$ than the through-the-thickness thermal diffusivity. For thermally anisotropic materials the diffusivity should include the anisotropy factor A in the exponential term, while for the thermally isotropic ones A = 1 in Eq. (7). The exponential term in Eq. (7), which multiplies the 1D terms, accounts for the physics of the diffusion of heat from the edge of the circular defect to the center, at distance $D/2$ away. In practice, Eq. (7) can be used to provide the temperature rise at any distance from the edge of the defect. It is assumed that the defect edge acts as a heat sink, sweeping away heat proportional to $e^{-\frac{(D/2)^2}{4\alpha A t}}$. The temperature contrast $T_c(h,t)$ on the surface of the material is obtained as follows:

$$T_c(h,t) = T_{d1}(h,t) - T_{nd}(h,t) = \left[T_d(h,t) - T_{nd}(h,t)\right]\left(1 - e^{-\frac{(D/2)^2}{4\alpha A t}}\right). \qquad (8)$$

The temperature contrast at the surface over a defective region is negative, it decreases with time until it reaches a minimum, after which it increases tending to zero. A thermal contrast image of the defect will be obtained, only if (i) the magnitude of the minimum temperature contrast is significantly above the noise level of the IR camera (typically 0.02 K), and (ii) the minimum contrast time is long enough to be recorded by the camera (typical frame rate 60 Hz). Examples of thermal images, along with further discussion, will be presented in Section 3. Effects of defect opening must also be accounted for, as real defects have a finite opening that may range from less than a μm to several mm. The thermal barriers presented by such defects are strongly dependent on defect opening and the thermal properties of the host material. Defects are usually treated as *thermal contact resistances*, $R = l_d / k_d$, where l_d is the *defect opening* and k_d is the thermal conductivity of the material filling the defect (usually it is assumed that defects are air filled). In a previous work from Patel et al. [23] on thermal wave interference an expression was obtained for the thermal reflectivity of a defect represented as a thermal contact resistance. That is:

$$\Gamma = \frac{Rk\sigma}{2 + Rk\sigma}. \qquad (9)$$

In the above equation, σ is the thermal wave number equal to $(1+i)/\mu$, where μ is the *thermal diffusion length*. The quantity $2\sqrt{\alpha t}$ is equivalent to μ for transient thermal phenomena. Making use of this in Eq. (9), it leads to the following expression:

$$\Gamma = \frac{R\zeta}{2\sqrt{t} + R\zeta}, \qquad (10)$$

where $\zeta = \sqrt{k\rho c}$ is the *thermal effusivity* of the composite laminate (W $s^{1/2}$ m^{-2} K^{-1}). Eq. (10) shows an effective thermal reflectivity of a defect that is a function of its thermal contact resistance R and the thermal properties k, ρ, c, of the host material. The results of using this expression have been found to be in good agreement with numerical modeling studies of the effects of defect opening on temperature contrast from Saintey and Almond [24]. Expression (10) is used in Eqs. (6) and (7) to compute the temperature contrast of

defects of specified openings. The temperature contrast can change dramatically depending on the defect opening, so this is a very important parameter whose effects will be analyzed in Section 3.

2.1 Analytical Expression for Evaluating the Defect Depth

The possibility of obtaining from the model derived in the previous Section an approximate expression for evaluating analytically the defect depth will be explored in the present subsection. Considering in Eq. (5) only the first term in the summations in *m* i.e. *m* = 0, and in Eq. (6) only the first term in the summations in *m* and two terms in the summations in *n*, i.e. *m* = 0 and *n* = 0, 1, then the temperature contrast $T_c(h,t)$ can be rewritten as:

$$T_c(h,t) = \left[T_d(h,t) - T_{nd}(h,t)\right]\left(1 - e^{-\frac{(D/2)^2}{4\alpha A t}}\right) = \frac{Q_0}{4\pi k t}\left[\Gamma e^{-\frac{(h+2d)^2}{4\alpha t}} + \Gamma e^{-\frac{(2L-h+2d)^2}{4\alpha t}} - \Gamma e^{-\frac{h^2}{4\alpha t}} - \Gamma e^{-\frac{(2L-h)^2}{4\alpha t}} - \Gamma^2 e^{-\frac{(h+2d)^2}{4\alpha t}} - \Gamma^2 e^{-\frac{(2L-h+2d)^2}{4\alpha t}}\right]\left(1 - e^{-\frac{(D/2)^2}{4\alpha A t}}\right) \quad (11)$$

Neglecting the second and the sixth terms on the right-hand side of Eq. (11), an approximate expression for the temperature contrast is obtained as follows:

$$T_c(h,t) = -\frac{Q_0}{4\pi k t}\Gamma\left[e^{-\frac{h^2}{4\alpha t}} + e^{-\frac{(2L-h)^2}{4\alpha t}} + \Gamma e^{-\frac{(h+2d)^2}{4\alpha t}} - e^{-\frac{(h+2d)^2}{4\alpha t}}\right]\left(1 - e^{-\frac{(D/2)^2}{4\alpha A t}}\right). \quad (12)$$

As previously discussed, the temperature contrast on the surface of the laminate over a defective area reaches a minimum $T_c = T_{c_{\min}}$ at a certain time $t = t_{\min}$ after the pulsed heat excitation has been released by the SMA wire. Assuming known material and defect thermal properties, geometry of the sample and defect diameter and opening, and substituting Γ with the expression in Eq. (10) and the values $T_c = T_{c_{\min}}$ and $t = t_{\min}$ derived from the experimental results in Eq. (12), then the following quadratic equation in the defect depth *d*, the only remaining unknown, is obtained:

$$d^2 + hd + \left(\frac{h}{2} - q_{18}\right)\left(\frac{h}{2} + q_{18}\right) = T_{c_{\min}}, \quad (13)$$

with solutions:

$$d_1 = q_{18} - \frac{h}{2}, \quad (14a)$$

$$d_2 = -\frac{h}{2} - q_{18}. \quad (14b)$$

For clarity, the values of q_{18} and the other coefficients in Eqs. (14a) and (14b) are reported in the Appendix. Only the positive solution d_1 in Eq. (14a) makes physical sense, and can be used to evaluate analytically the defect depth, assumed known all other parameters.

3. ANALYTICAL AND EXPERIMENTAL RESULTS

According to Section 2, this section presents the results of the analytical model and the approximate expression for evaluating analytically the defect depth as well as the experimental data. The analytical model was implemented in MATLAB [25]. The experimental results are for a four-ply laminated composite plate with orientations [0, 90, 90, 0] obtained from a composite T700/M21 unidirectional prepreg with fiber volume fraction $\approx$ 57-59%. The dimensions of the plate were 10 x 6 0.55 mm^3 (width x height x thickness). A NiTi SMA wire with a diameter of 350 μm was positioned between the 3rd and the 4th plies, while the presence of a defective area was modelled using a 1 cm^2 Teflon patch of $\approx$ 0.05 mm thickness. The inclusion of Teflon inserts is a well-known technique for introducing artificial in-plane delaminations in a laminate composite structure [15, 21, 26].

A pulse of *electric potential difference* ΔV was applied at the ends of the SMA wire in order to induce resistive heating in the component under test for a short heating period. The effects of the heating were then captured by the thermal camera in a thermographic system. The thermal camera was an InSb electrically cooled infrared camera with a noise-equivalent temperature difference of $\approx$ 18-25 mK and a resolution of 320 x 240 pixels (width x height). The camera was used at a frame rate of 50 Hz. The heating period was varied in the experiments between 10-50 ms in steps of 10 ms in order to characterise the impulsive nature of the analytical model. A ΔV of 2V was applied in all tests. An electrical resistance of 2.5 Ω was measured in the SMA wire. All tests were conducted at ambient temperature ($\approx$ 25). Figure 2 shows a comparison between the infrared images of the experimental data for the 30 ms heating period at different time instants after the impulsive heating excitation (which in this case occurred at t = 3.1 s).

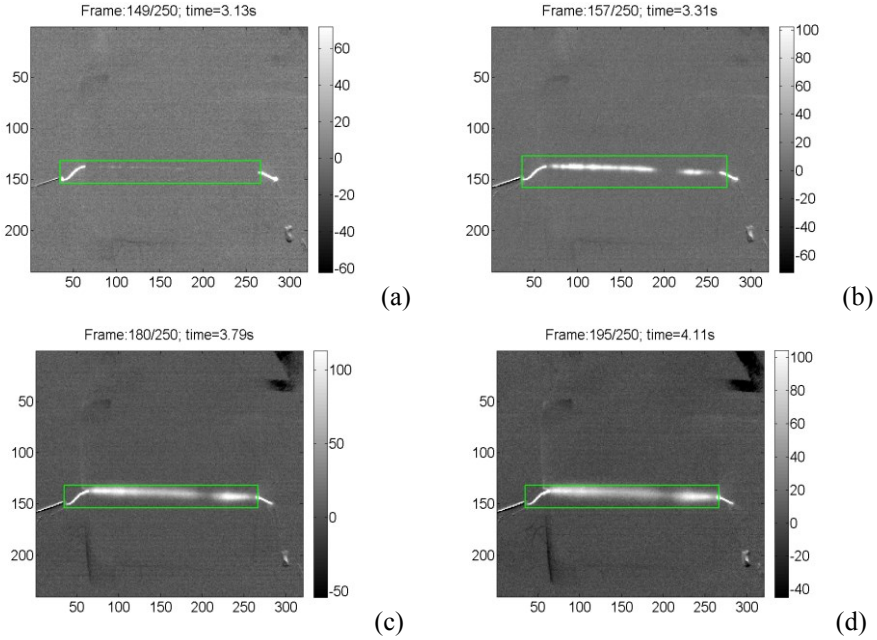

Figure 2 Comparison between the infrared images for the experimental data for the 30 ms heating period at different time instants after the impulsive heating excitation: 0.02 s (a), 0.18 s (b), 0.64 s (c) and 0.94 s (d).

Background subtraction was applied to the images in figure (2) between the pre-excitation and post-excitation thermal images. Then, the images were smoothed locally using simple moving average and the digital levels of the visualized thermal images were also rescaled based on a user selectable *region of interest* (ROI), which is represented by a green rectangle in the figures (2a) to (2d). Figure (2a) refers to the thermal image at a time

immediately after the pulsed heat excitation, while figure (2b) is for a time t = 0.18 s after the pulsed excitation where the temperature contrast reaches its minimum value. The presence of the patch is clearly visible in figure (2b) as a break in the temperature rise in the thermal image. Figures (2c) and (2d) show how at times much later there is a temperature rise also on the surface area over the patch caused by heat diffusion both through and around the defective area. Figure (3a) shows the results for the experimental data for the 30 ms heating period. All graphs in figure (3a) are plotted starting from when the SMA wire starts heating, after ΔV has been applied, and were smoothed locally using simple moving averaging. The non-defective temperature rise is being measured on the surface of the plate in a small non-defective area directly on top of the SMA wire, so that it is uniform as much as possible. After the initial rise the non-defective temperature decreases because of the effects of thermal convection towards the air surrounding the sample and thermal conduction in-plane to the SMA wire. The temperature is given in digital levels. The non-defective temperature increases by $\approx$ 96 digital levels. The defective temperature rise is measured on the surface of the plate in a small defective area directly on top of the SMA wire, so that, again, it is uniform as much as possible. The graph of the defective temperature rise takes into account not only the effects of thermal diffusion through the defect, but also the effects of lateral thermal diffusion around the defect. The defective temperature rise is of $\approx$ 30 digital levels. The temperature contrast in figure (3a) is negative reaching a minimum at 0.20 s. The temperature contrast reduction is of $\approx$ 100 digital levels.

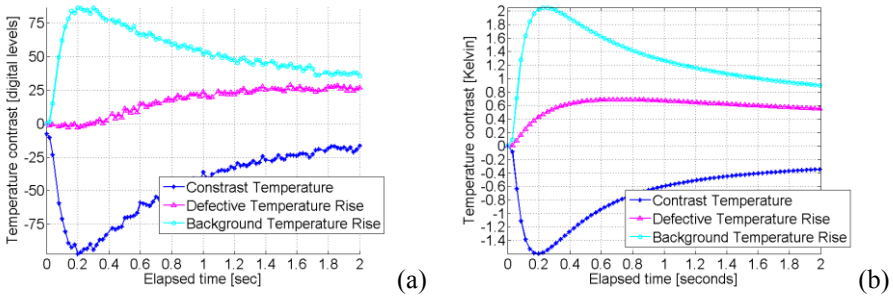

Figure 3 Results from Eq. (8) compared against the experimental ones for the 30 ms heating period. Figure (3a) shows the experimental results where $T_{c_{\min}} = -96.9$ digital levels and $t_{\min} = 0.20$ s. Figure (3b) illustrates the results from the analytical model in Eq. (8) where $T_{c_{\min}} = -1.60$ K and $t_{\min} = 0.19$ s.

Figure (3b) shows the results from the analytical model [Eq. (8)] corresponding to the experimental data in figure (3a). For comparison with the experimental data, the analytical model is computed using a plate thickness L of 0.55 mm and a wire depth h of 0.4125 mm. A defect depth d of 0.1375 mm and a defect diameter D of 10 mm were assumed. Furthermore, to allow for imperfections in the bonding between patch and host material during the manufacturing process, it was assumed that the defect opening was 100 μm and that the defect filler was air. The thermal properties utilized for the laminated composite plate are given in table 1.

Table 1. Thermal properties of CFRP used in the analytical model.

k [Wm^{-1} K^{-1}]	c [J kg^{-1} K^{-1}]	ρ (kg m^{-3})	α [m^2 s^{-1}]	A
0.5	1200	1700	5.88	4

The values in table 1 were derived by fitting the results of the analytical model to those of the experimental data. In particular, the procedure consisted in two stages. In the first stage, the through-the-thickness thermal diffusivity α was derived by fitting the temperature contrast obtained experimentally to the one computed using Eq. (8) for a value of $\Gamma = 1$, which corresponds to a null contribution of the defective temperature rise.

Then, the thermal anisotropy A was derived by fitting the defective temperature rise obtained experimentally to the one computed from Eq. (7). The fitting was performed at a distance $D/2$ = 2.5 mm from the edge of the defect, where the lateral diffusion was seen to be especially strong in the thermal images. The non-defective and defective temperatures in figure (3a) are constructed using, respectively, $m = 0,\ldots,10$ in Eq. (5) and $m = 0,\ldots,10$ and $n = 0,\ldots,10$ in Eq. (6). The temperature contrast computed by the analytical model agrees quite well the experimental results in figure (3a), with the model predicting a trough in the temperature contrast of -1.60 K at 0.19 s. In table 2 the results predicted by the analytical model (M) [Eq. (8)] and its approximate expression (AM) [Eq. (12)] for the minimum contrast time t_{min} are compared against the experimental ones for 10 ms, 20 ms, 30 ms, 40 ms and 50 ms heating periods.

Table 2. Results predicted by the analytical model (M) [Eq. (8)] and its approximate expression (AM) [Eq. (12)] for the minimum contrast time t_{min} compared against the experimental ones for 10 ms, 20ms, 30ms, 40ms and 50ms heating periods.

	M	**AM**	**10 ms**	**20 ms**	**30 ms**	**40 ms**	**50 ms**
$t_{\min}$ **[s]**	0.19	0.20	0.20	0.24	0.20	0.18	0.24

Figure (4a) shows the temperature contrast versus elapsed time curves computed using the analytical model [Eq. (8)] for four defect openings [i.e. the parameter R in Eq. (10)]: wide open (2.5 cm), 100 μm, 10 μm and 1 μm, holding fixed all other parameters. These curves are compared with a noise margin of 0.05 K that is taken as being the minimum temperature contrast necessary to produce a useful thermal image of a defect. The results change significantly depending on the defect opening being considered, as was also found in Saintey and Almond [24], with the minimum contrast temperature and time in these curves increasing with defect depth. Figure (4b) shows the temperature contrast versus elapsed time curves for the same parameters in figure (4a) but doubling the defect depth to 0.2750 mm. In this case for the defect opening 100 μm the minimum temperature contrast is $T_{c_{\min}} = -1.66$ K at time $t_{\min} = 0.21$ s which are respectively $\approx$ 3% and $\approx$ 10% greater than for the same curve in figure (4a), which gives an indication of the parameter sensitivity of the minimum contrast temperature and position for changes in the defect depth. In figure 4 defects with all of the four openings exceed the noise margin, indicating SMArt thermography to be suitable as a NDE technique for the inspection, but the sensitivity of the contrast to defect opening is evident, with the temperature contrast curve for the 1 μm opening size just above the noise margin.

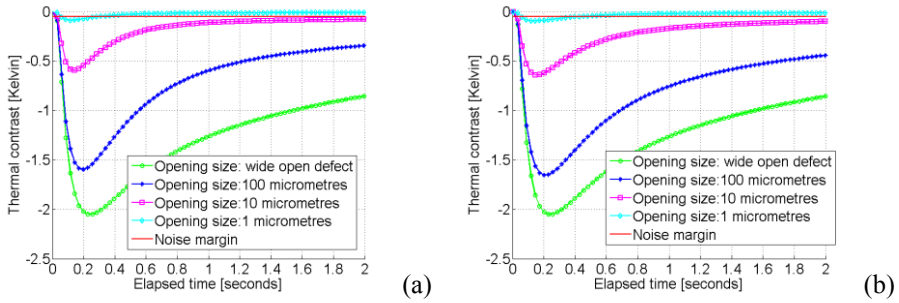

Figure 4 Temperature contrast versus elapsed time curves computed using Eq. (8) for four defect openings: wide open (2.5cm), 100µm, 10µm and 1µm, and for two different defect depths: 0.1375 mm (a) and 0.2750mm (b).

Figure (5) shows the temperature contrast versus elapsed time computed using the approximate expression [Eq. (12)] for the same parameters used in figure (3b). In this case the minimum temperature contrast is

$T_{c_{\min}} = -1.61$ K at time $t_{\min} = 0.20$ s. Substituting these values into the expression of d_1 given by Eq. (14a), the correct answer for the defect depth, i.e. 1.375 x 10^{-4} m, is obtained.

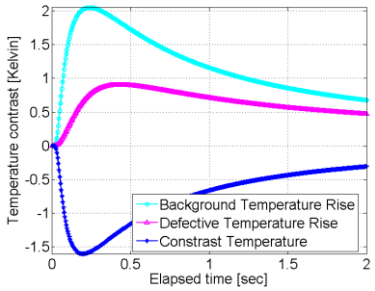

Figure 5 Temperature contrast versus elapsed time computed using Eq. (12) for the same parameters used in figure (3b).

Figure (6) shows the sensitivity of minimum contrast temperature and time to variations in the defect depth using the approximate expression [Eq. (12)] for the two defect depths in figure (4). Minimum contrast temperature and time were not found to be very sensitive to variations of the defect depth using this approximate expression, as a ≈ 50% variation in defect depth causes only a couple of percentage points variation in these parameters. For this reason, small errors in the minimum contrast temperature and time might produce large errors in the defect depth when computed analytically using Eq. (14).

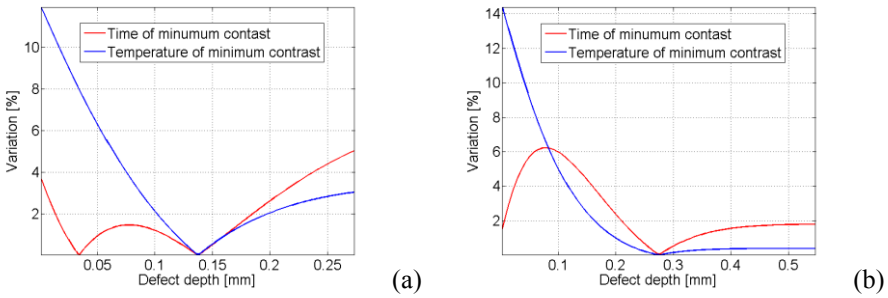

Figure 6 Sensitivity of minimum contrast temperature and time versus defect depth using Eq. (12) for the two defect depths in figure 4.

3.1 Analytical and Experimental Results for the Defect Depth Assessment

Figure (7) shows the results predicted for the defect depth d by d_1 in Eq. (14) from the experimental data for the 10 ms, 20 ms, 30 ms and 40 ms heating periods. These graphs are plotted against the width of the plate, as this is the dimension along which the SMA wire is running through the plate (i.e. the abscissas in figure 2). Contrast figure (7a) to (7d) to figure (2b) to have a visual comparison of the defect size and location. The differences between the maximum predicted value in figures (7a) to (7d), compared to the assumed value ≈ 0.1375 mm, range between 1-7%.

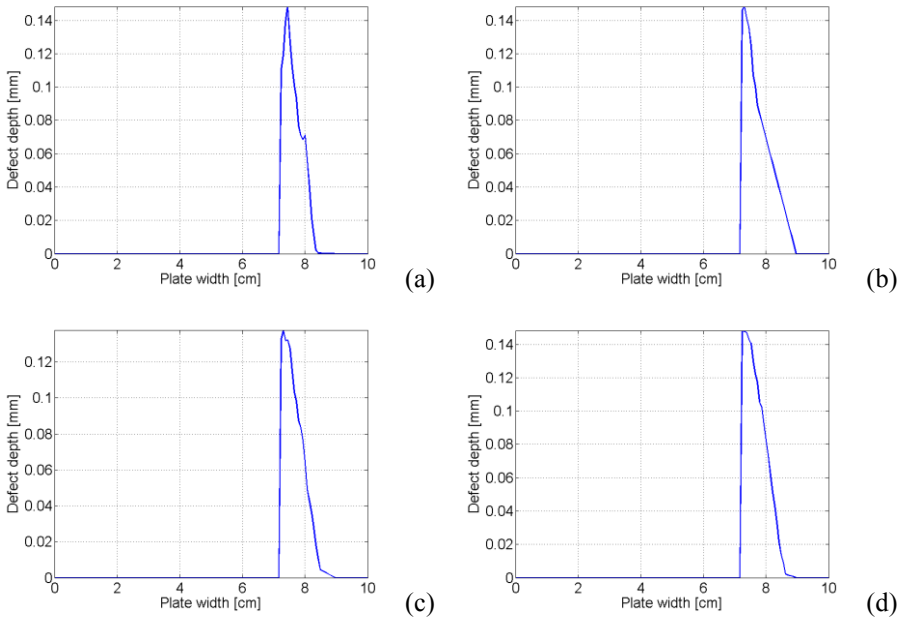

Figure 7 Results predicted for the defect depth *d* by d1 in Eq. (14) from the experimental data for the 10ms, 20ms, 30ms and 40ms heating periods. These graphs are plotted against the width of the plate, as this is the dimension along which the SMA wire is running through the plate.

The defect depth was evaluated using the following procedure:

1. Temperature contrast curves were generated from the experimental data, using the same non-defective temperature rise computed at a small area located on top of the SMA wire, and were smoothed locally using simple moving averaging.
2. The defect depth was then evaluated at each location along the wire employing the expression for d_1 in Eq. (14) where the minimum temperature $T_{c_{\min}}$ and time $t_{\min}$ are computed from the temperature contrast curve of the experimental data. There will be small positive or negative values of contrast temperature for all non-defective regions compared to the reference one, because of local differences in the heat conduction phenomena and noise in the thermographic system. These can be safely discarded in three ways:
    a. by setting to zero the defect depth when the contrast temperature is found to be positive;
    b. by setting to zero the defect depth when the contrast temperature is found to be negative, but is far away from the location of the defect (which is assumed to have been previously estimated from the thermal images);
    c. by removing from the results any complex or negative values of defect depth.

    In fact, by construction, Eq. (14) will produce a real positive, physically meaningful result for the defect depth only for values of contrast temperature and time that fit closely the curve in figure (5).
3. Finally, previously discarded results for the defect depth were reconstructed using *inpainting* techniques, which aim at filling-in holes in digital data by propagating surrounding data (e.g. [27]), the only condition being that the defect depth on the boundaries of the plate should be zero.

In figures (5), (6) and (7) the defect diameter D is assumed to have been estimated precisely from the thermal images. In real applications a component would carry a grid of SMA wires, at known distances and depths, which can be used to estimate the extent of the damage, hence the value of the diameter to be used in the expression for d_1 in Eq. (14). A methodology for estimating the size of the internal damage based on the *a-priori* knowledge of the inter-wire distance and length is discussed in Pinto et al. [15]. Despite good agreement with the experimental data (errors ranging between 1-7%), some limitation must be highlighted. The analytical expression for the defect depth assumes known material and defect thermal properties, geometry of the sample and defect diameter and opening. While the defect diameter can be estimated from the thermal images, it is not possible to estimate the defect opening. All that is feasible is to evaluate the defect depths for a range of defect openings for a specific application. Furthermore, minimum contrast temperature and time using the approximate expression were not found to be very sensitive to large variations of the defect depth, but highly dependent on defect opening.

4. CONCLUSIONS

The aim of this paper was to develop an analytical model for pulsed thermography to predict analytically the depth of flaws/damages within composite materials. This model can also be used to predict the temperature contrast on the surface of the laminate, accounting for defect depth, size and opening, thermal properties of material and defect filler, thickness of the component, and intensity of the excitation energy. The results showed that the analytical model gives good predictions compared to experimental data (errors ranging between 1-7%). The proposed approach relies on the knowledge of the defect opening. This paper is one of the first pioneering work showing the use thermography as a quantitative non-destructive where defect size and depth can be assessed.

5. APPENDIX

The coefficients used to calculate the defect depth in Eq. (13) are here reported as follows:

$$q_1 = \left(e^{\frac{D^2}{\alpha A t_{\min}}} \right)^{\frac{1}{16}}; \quad q_2 = e^{\frac{L^2}{\alpha t_{\min}}}; \quad q_3 = \left(e^{\frac{h^2}{\alpha t_{\min}}} \right)^{\frac{1}{4}}; \quad q_4 = e^{\frac{Lh}{\alpha t_{\min}}};$$

$$q_5 = 2Q_0 R\sqrt{t_{\min}}\zeta q_1 q_2; \quad q_6 = 2Q_0 R\sqrt{t_{\min}}\zeta q_1 q_4; \quad q_7 = Q_0 R^2 \zeta^2 q_1 q_2;$$

$$q_8 = Q_0 R^2 \zeta^2 q_1 q_4; \quad q_9 = 16\pi T_{c_{\min}} k t_{\min}^2 q_1 q_2 q_3; \quad q_{10} = q_5/q_1;$$

$$q_{11} = q_6/q_1; \quad q_{12} = q_7/q_1; \quad q_{13} = q_8/q_1; \quad q_{14} = \frac{R^2\zeta^2 q_9}{4t_{\min}}; \quad q_{15} = R\zeta q_9 t_{\min}^{3/4};$$

$$q_{16} = q_5 + q_6 + q_7 + q_8 + q_9 - q_{10} - q_{11} - q_{12} - q_{13} + q_{14} + q_{15};$$

$$q_{17} = q_{10} - q_5; \quad q_{18} = \frac{1}{2}\left[h^2 - 4\alpha t_{\min} \log\left(-\frac{q_{16}}{q_{17}} \right) \right]^{\frac{1}{2}}$$

REFERENCES

[1] J. Milne, W. Reynolds, The non-destructive evaluation of composites and other materials by thermal pulse video thermography, in: 1984 Cambridge Symposium, International Society for Optics and Photonics, 1985, pp. 119-122.

[2] S. M. Shepard, Advances in pulsed thermography, in: Aerospace/Defence Sensing, Simulation, and Controls, International Society for Optics and Photonics, 2001, pp. 511-515.

[3] V. V. Bolotin, Delaminations in composite structures: its origin, buckling, growth and stability, Composites Part B: Engineering 27 (2) (1996) 129-145.

[4] U. Polimeno, M. Meo, Detecting barely visible impact damage detection on aircraft composites structures, Composite Structures 91 (4) (2009) 398-402.

[5] F. Ciampa, M. Meo, "Nonlinear elastic imaging using reciprocal time reversal and third order symmetry analysis," J. Acoust. Soc. Am. 131 (6), (2012) 4316-4323.

[6] X. Maldague, Nondestructive Evaluation of Materials by Infrared Thermography, 1st Edition, Springer, London, 1993.

[7] D. P. Almond, S. Lau, Edge effects and a method of defect sizing for transient thermography, Applied physics letters 62 (25) (1993) 3369-3371.

[8] S. Lau, D. Almond, J. Milne, A quantitative analysis of pulsed video thermography, NDT & E International 24 (4) (1991) 195-202.

[9] N. Ludwig, P. Teruzzi, Heat losses and 3d diffusion phenomena for defect sizing procedures in video pulse thermography, Infrared Physics & Technology 43 (3{5) (2002) 297-301.

[10] D. P. Almond, S. G. Pickering, An analytical study of the pulsed thermography defect detection limit, Journal of Applied Physics 111 (9) (2012) 093510.

[11] D. P. Almond, S. G. Pickering, Analysis of the defect detection capabilities of pulse stimulated thermographic NDE techniques, AIP Conference Proceedings 1581 (1) (2014) 1617-1623.

[12] S. Lau, D. Almond, P. Patel, Transient thermal wave techniques for the evaluation of surface coatings, Journal of Physics D: Applied Physics 24 (3) (1991) 428.

[13] D. P. Almond, P. Patel, Photothermal science and techniques, 1st Edition, Vol. 10 of Chapman & Hall Series in Accounting and Finance (Book 10), Springer, London, 1996.

[14] C. Bennett Jr, R. Patty, Thermal wave interferometry: a potential application of the photoacoustic effect, Applied Optics 21 (1) (1982) 49-54.

[15] F. Pinto, F. Ciampa, M. Meo, U. Polimeno, Multifunctional smart composite material for in situ NDT/SHM and de-icing, Smart Materials and Structures 21 (10) (2012) 105010.

[16] J. P. Thomas, M. A. Qidwai, Mechanical design and performance of composite multifunctional materials, Acta Materialia 52 (8) (2004) 2155-2164.

[17] S. L. Angioni, M. Meo, A. Foreman, Impact damage resistance and damage suppression properties of shape memory alloys in hybrid composites-a review, Smart Materials and Structures 20 (1) (2011) 013001.

[18] H. Nagai, R. Oishi, Shape memory alloys as strain sensors in composites, Smart materials and structures 15 (2) (2006) 493.

[19] Y. Xu, K. Otsuka, H. Nagai, H. Yoshida, M. Asai, T. Kishi, A SMA/CFRP hybrid composite with damage suppression effect at ambient temperature, Scripta Materialia 49 (6) (2003) 587-593.

[20] F. Pinto, F. Maroun, M. Meo, Material enabled thermography, NDT & E International 67 (0) (2014) 1-9.

[21] F. Pinto, F. Ciampa, U. Polimeno and M. Meo, In situ damage detection in SMA reinforced CFRP, Proc. SPIE 8345, Sensors and Smart Structures Technologies for Civil, Mechanical, and Aerospace Systems 2012, 83452V.

[22] H. S. Carlslaw, J. C. Jaeger, Conduction of Heat in Solids, 2nd Edition, Oxford University Press, 1959.

[23] P. Patel, D. Almond, H. Reiter, Thermal-wave detection and characterisation of sub-surface defects, Applied Physics B 43 (1) (1987) 9-15.

[24] M. Saintey, D. P. Almond, Defect sizing by transient thermography. ii. a numerical treatment, Journal of Physics D: Applied Physics 28 (12) (1995) 25-39.

[25] MATLAB, version 8.0.0.783 (R2012b), The MathWorks Inc., Natick, Massachusetts, 2012. URL www.mathworks.com

[26] F. Ciampa, S. Pickering, G. Scarselli, and M. Meo, Nonlinear damage detection in composite structures using bispectral analysis, in: SPIE Smart Structures and Materials+ Nondestructive Evaluation and Health Monitoring, International Society for Optics and Photonics, 2014, pp. 906402-906402.

[27] D. Garcia, Robust smoothing of gridded data in one and higher dimensions with missing values, Computational statistics & data analysis 54 (4) (2010) 1167-1178.